Investigating the solid-gas phase reaction between WO$_3$ powder, NH$_3$ and H$_2$O vapors to prepare ammonium paratungstate

Dávid Hunyadi[1*], Imre Miklós Szilágyi[1,2], Attila L. Tóth[3], Eszter Drotár[4], Tamás Igricz[5], György Pokol[1]

[1]Department of Inorganic and Analytical Chemistry, Budapest University of Technology and Economics, H-1111 Budapest, Szt. Gellért tér 4. Hungary

[2]Materials Structure and Modeling Research Group of the Hungarian Academy of Sciences, Budapest University of Technology and Economics, H-1111 Budapest, Szt. Gellért tér 4. Hungary

[3]Research Institute for Technical Physics and Material Science, Hungarian Academy of Sciences, H-1121 Konkoly-Thege út 29-33. Budapest, Hungary

[4]Institute of Materials and Environmental Chemistry, Hungarian Academy of Sciences, H-1117 Budapest, Magyar tudósok körútja 2.

[5]Department of Organic Chemistry and Technology, Budapest University of Technology and Economics, H-1111 Budapest, Budafoki út 8. Hungary

*E-mail address: david.hunyadi89@gmail.com; Tel: +36-1-463-4141

Abstract

The solid-gas phase heterogeneous reaction between tungsten oxide powder, ammonia and water vapors was studied with the aim of preparing ammonium paratungstate (APT, $(NH_4)_{10}[H_2W_{12}O_{42}] \cdot xH_2O$ (X=4,10)). The effects of the composition, crystal structure and particle size of the WO_3 powder were investigated along with the effect of the partial pressure of ammonia and water vapor on the products. The as-prepared APT was characterized with powder XRD, FTIR, Raman, SEM, TEM and TG/DTA-MS measurements. At 43,40 kPa and 12,23 kPa ammonia partial pressures after one day two partially reduced intermediates, i.e. W_5O_{14} and $(NH_4)_2W_2O_7 \cdot 0.5H_2O$, were identified, which transformed into APT·$4H_2O$ in 30 days with a yield of almost 100 %. $(NH_4)_2W_2O_7 \cdot 0.5H_2O$ was produced for the first time ever, while for W_5O_{14} this was a new preparation route, as it was only produced in great vacuum at high temperature before. At 1.56 kPa ammonia partial pressure APT·$10H_2O$ was also a product of the reaction. At lower ammonia partial pressures the reaction was very slow, and only small changes were detected in the structure after 30 days. The results showed that this novel synthesis of APT is not sensitive to the reaction conditions, in contrast to the previously only available wet chemical crystallization process. According to the measurements, the as-produced APT is equivalent to the commercial ones. As an additional feature, our method is capable to yield APT nanoparticles for the first time, which is important for both research and industry due to the greater surface area.

Keywords

1. Introduction

The ammonium paratungstate (APT), $(NH_4)_{10}[H_2W_{12}O_{42}]\cdot xH_2O$ (X=4,7,10) is the most important starting material in the tungsten industry, where usually its most stable $APT\cdot 4H_2O$ form is used [1]. From APT tungsten oxides, tungsten carbides or tungsten metal can be prepared. Among others, tungsten oxides are widespread catalysts [2-5], photocatalysts [6-10] and gas sensors [11-18]. Tungsten carbide products are also used as catalysts [19,20], but their another important application field is being the hard component in cutting and drilling tools [21-23]. Tungsten metal is applied in lightning industry [1, 24-28], steel metallurgy [29,30], sporting and medical equipments [31,32] and electronics [32].

Today APT is produced by the wet chemical process [1], which is a multi-step method. The first step is the alkaline digestion, when the tungsten content is extracted from the tungsten ore concentrates, scrap metal or oxides [33]. The next step is the purification of the gained sodium tungstate solution. The type and concentration of the contaminants can vary; the typical contaminating ions are silicate, phosphate, arsenate, molybdate, fluoride, lead, bismuth and aluminum. The separation is started with silica precipitation, where the silica, phosphate and fluoride ions are separated by adding aluminum sulfate or magnesium sulfate to the solution. After that sulfide-forming cations like arsenic, molybdenum, antimony, bismuth, cobalt, etc are separated by adding sodium sulfide to the solution [33]. The third step is the ion exchange, when the sodium ions are replaced by ammonium ions. First an organic solvent is added with phase transfer catalyst to the aqueous solution, so that the tungstate content is moved to the organic phase. After that aqueous ammonia solution is added to the separated organic phase. At the end of this step an aqueous solution of ammonium isopolytungstate is obtained [34,35], from which the APT is produced by crystallization. During the evaporation of the solution, ammonia and water are volatilized. As the pH of the solution decreases and the WO_3 concentration increases at the same time, paratungstate A ion, $[HW_6O_{21}]^{5-}$ is formed,

which transforms into paratungstate B ion, $[H_2W_{12}O_{42}]^{10-}$ in an equilibrium reaction. The ammonium salt of the paratungstate B ion has the lowest solubility at these conditions, hence $(NH_4)_{10}[H_2W_{12}O_{42}]\cdot 4H_2O$ (APT·$4H_2O$) crystallizes [36,37].

Because of its importance the production of APT has been studied for several decades, therefore the wet chemical process has been explored in detail. Nevertheless it has several disadvantages, e.g. it is very sensitive to the conditions, especially to the pH. In addition, the process has a large chemical and energy requirement [1].

The solubility of WO_3 is good in concentrated alkaline and ammonia solution. Therefore it is also used in the wet chemical process to produce APT [1]. However, it has been unknown, how NH_3 and H_2O vapors can react with WO_3, and whether they can digest it. Our main goal was to explore this reaction (Fig. 1).

Therefore, in the present study APT was produced with a solid-gas phase heterogeneous reaction between WO_3 powder, NH_3 and H_2O vapors. The effects of the reaction conditions on the products were examined: the composition, crystal structure and particle size of the WO_3 powder and the partial pressure of the ammonia vapor. Then the as-prepared APT was characterized thoroughly, by powder X-ray diffraction (XRD), Fourier transform infrared spectroscopy (FTIR), Raman spectroscopy, transmission electron microscopy (TEM), scanning electron microscopy (SEM), and thermal analysis (TG/DTA-MS). Based on our results the properties of the as-obtained APT are identical to the commercial APT materials, also this is the only method to prepare nanosize APT.

2. Experimental

2.1 Preparation of the WO₃ starting materials

As a reference material, commercial ammonium paratungstate (APT·4H$_2$O) was obtained from H. C. Starck GmbH. WO$_3$ powders prepared from the reference APT and from hexagonal ammonium tungsten bronze (HATB, (NH4)$_{0.33-x}$WO$_{3-y}$) were used as precursors in the solid-gas phase reactions. HATB was obtained by heating APT at 400 °C in H$_2$ for 6h [38]. The precursor tungsten oxides with different compositions (oxidized or partially reduced), structures (monoclinic (m-WO$_3$) or hexagonal (h-WO$_3$)) and particle sizes (70-90 or 100-300 nm) were prepared by thermal decomposition from APT or HATB by controlling the annealing temperature and atmosphere [39]. The details of preparations are summarized in Table 1.

According to SEM images (Fig. 2), the precursor tungsten oxides (**1**, **2**, **5-8**) produced from APT consisted of ca. 100-300 nm particles (Fig. 2a), which aggregated into 30-100 μm blocks (Fig. 2b). While the precursor oxides (**3**, **4**, **9-11**) obtained from HATB were built up by ca. 70-90 nm particles (Fig. 2c), which also aggregated into 30-200 μm blocks (Fig. 2d).

2.2 Solid-gas phase reactions

The reactions between the precursor tungsten oxide powders and the NH$_3$ and H$_2$O vapors were carried out at room temperature in a sealed plastic box. WO$_3$ powder and aqueous ammonia solution were placed separately into the box, where the reagents were able to react only via the gas phase. The partial pressures of ammonia and water vapor were controlled by varying the concentration of ammonia in the solutions (Table 1). The equilibrium partial pressure of NH$_3$ and H$_2$O vapors values were calculated from the concentrations of the aqueous solutions [40]. Using precursors **1** to **4** the effects of the composition and crystal structure of the tungsten oxides were investigated. From precursors **5** to **11** the effects of the particle size of the powders and the partial pressure of the ammonia were studied.

In each reaction 500 mg WO_3 powder and 25 ml aqueous ammonia solution were used. The yield of the reactions was calculated from the mass difference before and after the reaction.

2.3 Analytical methods used for the characterization

Powder XRD patterns were recorded on a PANalytical X'pert Pro MPD X-ray diffractometer using Cu K_α radiation.

FTIR spectra were measured by an Excalibur Series FTS 3000 (Biorad) FTIR spectrophotometer in the range of 400-4000 cm^{-1} in KBr pellets.

Raman spectra were measured by a Jobin Yvon Labram spectrophotometer equipped with an Olympus BX41 microscope in the range of 130-900 cm^{-1}. As exciting source Nd-YAG laser (532 nm) was used with 1 mW output.

The SEM images were recorded by a LEO-1550 FEG scanning electron microscope with a field emission cathode and InLens detector.

The TEM images were obtained by a FEI Morgagni 268D transmission electron microscope.

TG/DTA measurements were performed on an STD 2960 Simultaneous DTA/TGA (TA Instruments Inc.) thermal analyzer using a heating rate of 10 °C min^{-1} and Pt crucibles. The furnace was purged either with air or nitrogen atmospheres (130 ml min^{-1}). Evolved gas analytical (EGA) curves were recorded by a Thermostar GSD 200 (Balzers Instruments) quadrupole mass spectrometer (MS). A mass range between m/z = 1-64 was monitored through 64 channels in Multiple Ion Detection Mode (MID) with a measuring time of 0.5 s channel^{-1}. Further details of the TG/DTA-MS setup are described in other studies [41,42].

3. Results and discussion

3.1 XRD measurements

At first, the effects of the composition (**1** (oxidized m-WO$_3$), **2** (partially reduced m-WO$_3$)) and crystal structure (**3** (h-WO$_3$), **4** (m-WO$_3$)) of the precursor tungsten oxides were investigated. In case of these four reactions the partial pressure of ammonia was 43.40 kPa. The intermediate and final products were the same in the case of precursors **1**-**4**; thus, only the XRD patterns for precursor **4** are shown here (Fig. 3). The crystal structure changed already after 1 day, as new reflections appeared in the XRD pattern. After 1 week a multiphase mixture was obtained, and as one of the intermediate products W$_5$O$_{14}$ (PDF 07-2137) was identified. Also another intermediate was probably (NH$_4$)$_2$W$_2$O$_7$·0.5H$_2$O, this phase was not in the ICDD database, for its identification Na$_2$W$_2$O$_7$·0.5H$_2$O (PDF 10-4500) was used, which could has a similar crystal structure, since NH$_4^+$ and Na$^+$ ions can be in similar positions in the crystal structure due to their similar sizes [1]. The appearance of these phases is significant because, on the one hand, the (NH$_4$)$_2$W$_2$O$_7$·0.5H$_2$O phase was produced for the very first time. On the other hand, the W$_5$O$_{14}$ phase was only produced at high temperatures in vacuum before [43,44], so this reaction is a new preparation route. The (NH$_4$)$_2$W$_2$O$_7$·0.5H$_2$O and W$_5$O$_{14}$ intermediate phases transformed into APT after 30 days with a yield of almost 100 %. The powder composition had an effect on the quality of the product (Fig. 4), since APT with the highest degree of crystallinity was obtained from the partially reduced m-WO$_3$ precursor (**2**). This oxide has a distorted crystal lattice [39], thus it can be transformed more easily, and this might be the reason why the best quality APT was produced from this oxide. The second best quality APT was formed from the also slightly distorted hexagonal tungsten oxide precursor (**4**) [39]. From the more ordered monoclinic tungsten oxide precursors (**1**, **3**) less crystalline APT materials were prepared.

7

In the next series of experiments (**5-11**) the effects of the particle size of the tungsten oxides and the partial pressure of ammonia were studied. At 12.23 kPa ammonia partial pressure (**8**) the same reduced intermediate phases were observed as in the case of **1**-**4**; however, the structure of the intermediates was less crystalline. The reason for this was that the reducing effect of the ammonia vapor was smaller due to the lower ammonia pressure. After 30 days less crystalline APT sample was produced (Fig. 4).

At even lower ammonia partial pressures the effect of the particle size can be seen. At 1.56 kPa NH_3 partial pressure the precursor **6** (100-300 nm) transformed into $APT \cdot 10H_2O$ (PDF 55-0763), while the precursor **10** (70-90 nm) transformed into the expected $APT \cdot 4H_2O$. This is a significant result, because through this reaction a new way was found to prepare the $APT \cdot 10H_2O$ (Fig. 4).

At 0.77 kPa ammonia partial pressure and after 30 days of reaction, only tiny APT peaks were observed in the case of precursor **7** (100-300 nm), while the structure remained mostly m-WO_3. In contrast, precursor **11** (70-90 nm) transformed into APT to a greater extend (Fig. 4). The reason for this is that smaller particle size resulted in higher reaction speed.

At 0.15 kPa ammonia partial pressure and after 30 days, in the case of precursor **9** (70-90 nm) only very small APT peaks could be observed, while precursor **5** (100-300 nm) was unchanged, compared to the starting tungsten oxide. This suggests that if the partial pressure of the ammonia is too low, the reaction is too slow to induce significant changes in the structure (Fig. 4).

3.2 FTIR measurements

The ammonia and water adsorption on the surface of the oxide particles and then the incorporation into the crystal lattice was monitored by FTIR measurements (Fig. 5). Since the

APT with the best quality was prepared from precursor **2**, only FTIR results for **2** are presented here. The incorporation of H_2O and NH_3 can be seen after already one day. By increasing the reaction time, the intensity of water peaks at 1627 cm^{-1} (O-H deformation vibration) and 3360 cm^{-1} (O-H stretching vibration) and of NH_4^+ peaks at 1403 cm^{-1} (N-H deformation vibration) and 3139 cm^{-1} (N-H stretching vibration) increased. Below 1000 cm^{-1} the rearrangements of the W-O bonds can be seen as the tungsten oxide transformed into the intermediates (W_5O_{14}, $(NH_4)_2W_2O_7 \cdot 0.5H_2O$), and then these phases transformed into APT.

The FTIR spectrum of the as-produced APT matched the FTIR spectrum of the commercial APT. The peaks belonging to the paratungstate ion were observable mostly below 1000 cm^{-1}, i.e. the peak at 934 cm^{-1} was assigned to W=O vibrations, while the peaks at 700-900 cm^{-1} (702, 765, 818, 870 cm^{-1}) were explained by the W-O vibrations [45-47].

3.3 Raman measurements

As Fig. 6 shows, the Raman spectra of the as-produced and the commercial APT materials were the same. Around 950 cm^{-1} there are 3 overlapping peaks (948 cm^{-1}, 931 cm^{-1}, 915 cm^{-1}) which are assigned to the symmetric stretching of the W=O bonds. In the range of 800-900 cm^{-1} the asymmetric stretching of the W=O bonds can be seen, at 868 cm^{-1} there is a separated peak and 2 overlapping peaks (826 cm^{-1}, 800 cm^{-1}) [48,49]. The peaks at lower values (700-100 cm^{-1}) are from the bridging W-O-W bonds (676 cm^{-1}, 645 cm^{-1}, 570 cm^{-1}, 505 cm^{-1}, 385 cm^{-1}, 350 cm^{-1}, 316 cm^{-1}, 224 cm^{-1}, 206 cm^{-1}, 161 cm^{-1}, 119 cm^{-1}, 82 cm^{-1}, 69 cm^{-1}) [49].

3.4 SEM measurements

The intermediate phases with the best quality were obtained not from precursor **2**, but from **4**, thus only the SEM images belonging to **4** are discussed here. It can be seen that after 1 week of reaction a multiphase mixture was obtained, as the images showed different morphologies: fibrous and planar structures could be separated (Fig. 7a-b). There were 80-100 nm particles on the surface of the 1 μm thick fibers. Also there were ca. 200 nm particles on the 1.5 μm thick plates too.

The APT with the best quality was produced from precursor **2**. The images of the as-prepared APT (Fig. 7c-d) showed that it consisted of ca. 0.2-2 μm particles with flat surface, which aggregated into 20-100 μm blocks.

3.5 TEM measurements

The as-produced APT consisted of larger (0.8-1.6 μm) and smaller (40-300 nm) particles as well (Fig. 8a). In Fig. 8b nanosize (40-300 nm) APT particles can be seen. This result is remarkable, because to the best of our knowledge, APT with such small particle size has not been reported previously. Due to its greater surface area, APT nanoparticles are expected to be important in research and industry in the future.

3.6 Thermal decomposition of APT

The thermal decomposition sequence of the as-produced APT material in N_2 (Fig. 9) was identical to the previous results [1,27,38,50-55]. The decomposition of APT included several steps. Until ca. 120 °C APT lost its crystal water content in an endothermic reaction and a dehydrated APT formed. In the second decomposition step (150-210 °C), dry NH_3 was released, accompanied by an endothermic heat effect. Between 220-320 °C both NH_3 and

H_2O were released, and an amorphous phase formed in an endothermic reaction. Between 330-400 °C from this phase hexagonal ammonium tungsten bronze (HATB) (PDF 42-0452), $(NH_4)_{0.33-x}WO_{3-y}$ or h-WO_3 (PDF 33-1387) formed. Between 400-500 °C the as-formed HATB/h-WO_3 transformed in an exothermic reaction into the thermodynamically stable m-WO_3 (PDF 43-1035).

4. Conclusions

In this study the solid-gas phase heterogeneous reaction between tungsten oxide powder, ammonia and water vapors was investigated with the goal to produce APT. The effects of the composition (oxidized or partially reduced), crystal structure (monoclinic or hexagonal) and particle size (100-300 nm or 70-90 nm) of the WO_3 powders were examined along with the effect of the partial pressures of ammonia and water vapors. According to the results, this synthesis is simple and not sensitive to the reaction conditions, in contrast to the more complex and sensitive wet chemical process.

At 43.40 kPa and 12.23 kPa ammonia partial pressures the ammonia vapor first reduced the tungsten oxides, and partially reduced intermediate phases, i.e. W_5O_{14} and $(NH_4)_2W_2O_7 \cdot 0,5H_2O$, formed after 1 day. For these two materials a new synthesis route was found. After 30 days the intermediate phases transformed into APT with a yield of almost 100 %. At 1.56 kPa ammonia pressure APT was produced after 30 days without the partially reduced intermediate phases. Also at this pressure a new synthesis route was found for APT·$10H_2O$, since from the 100-300 nm precursor monoclinic tungsten oxide particles APT·$10H_2O$ was the main product. At 0.77 kPa and 0.15 kPa ammonia partial pressures the reaction was too slow to induce significant changes in the structure.

The as-prepared APT was characterized with powder XRD, FTIR, Raman spectroscopy and TG/DTA-MS measurements. These measurements proved that the as-prepared APT is equal to the commercial one. SEM and TEM images revealed that nanosize (40-300 nm) APT was produced for the first time, which can be important in research and industry due to its greater surface area.

5. References

[1]   E. Lassner, W.D. Schubert, Tungsten properties, chemistry, technology of the element, alloys, and chemical compounds, Kluwer Academic/Plenum Publishers, New York, 1999.

[2]   C. Hammond, J. Straus, M. Righettoni, S.E. Pratsinis, I. Hermans, Nanoparticulate tungsten oxide for catalytic epoxidations. ACS Catal. 3 (2013) 321-7.

[3]   C. Di Valentin, F. Wang, G. Pacchioni, Tungsten oxide in catalysis and photocatalysis: Hints from DFT. Topics Catal. 56 (2013) 1404-19.

[4]   G. M. Veith, A. R. Lupini, S. J. Pennycook, V. Alberto, L. Prati, N. J. Dudney, Magnetron sputtering of gold nanoparticles onto WO_3 and activated carbon. Catal Today 122 (2007) 248-53.

[5]   A. Phuruangrat, D. J. Ham, S. J. Hong, S. Thongtem, J. S. Lee, Synthesis of hexagonal WO_3 nanowires by microwave-assisted hydrothermal method and their electrocatalytic activities for hydrogen evolution reaction. J Mater Chem. 20 (2010) 1683-90.

[6]   I. M. Szilágyi, B. Fórizs, O. Rosseler, Á. Szegedi, P. Németh, P. Király, G. Tárkányi, B. Vajna, K. Varga–Josepovits, K. László, A. L. Tóth, P. Baranyai, M. Leskelä, WO_3 photocatalysts: influence of structure and composition. J Catal. 294 (2012) 119-27.

[7]   C. T. Lin, T. H. Tsai, Solution volume effect of photodegradation by 1-D WO_3 nanorods via microwave-assisted solvothermal heating under the UV irradiation. Asian J Chem. 25 (2013) 7098-102.

[8]   A. B. D. Nandiyanto, O. Arutanti, T. Ogi, F. Iskandar, T. O. Kim, K. Okuyama, Synthesis of spherical macroporous WO_3 particles and their high photocatalytic performance. Chem Eng Sci. 101 (2013) 523-32.

[9]   B. X. Liu, J. S. Wang, H. Y. Li, J. S. Wu, M. L. Zhou, T. Y. Zuo, Facile synthesis of hierarchical hollow mesoporous Ag/WO$_3$ spheres with high photocatalytic performance. J Nanosci Nanotech. 13 (2013) 4117-22.

[10]   E. Karacsonyi, L. Baia, A. Dombi, V. Danciu, K. Mogyorosi, L. C. Pop, G. Kovacs, V. Cosoveanu, A. Vulpoi, S. Simon, Z. Pap, The photocatalytic activity of TiO2/WO$_3$/noble metal (Au or Pt) nanoarchitectures obtained by selective photodeposition. Catal Today 208 (2013) 19-27.

[11]   I. M. Szilágyi, S. Saukko, J. Mizsei, A. L. Tóth, J. Madarász, G. Pokol, Gas sensing selectivity of hexagonal and monoclinic WO$_3$ to H$_2$S. Solid State Sci. 12 (2010) 1857-60.

[12]   I. M. Szilágyi, L. Wang, P. I. Gouma, C. Balázsi, J. Madarász, G. Pokol, Preparation of hexagonal WO$_3$ from hexagonal ammonium tungsten bronze for sensing NH$_3$. Mater Res Bull. 44 (2009) 505-8.

[13]   C. Balázsi, L. Wang, E. O. Zayim, I. M. Szilágyi, K. Sedlackova, J. Pfeifer, A. L. Tóth, P. I. Gouma, Nanosize hexagonal tungsten oxide for gas sensing applications. J Eur Ceram Soc. 28 (2008) 913-7.

[14]   I. M. Szilágyi, S. Saukko, J. Mizsei, P. Király, G. Tárkányi, A. L. Tóth, A. Szabó, K. Varga-Josepovits, J. Madarász, G. Pokol, Controlling the composition of nanosize hexagonal WO$_3$ for gas sensing. Mater Sci Forum 589 (2008) 161-5.

[15]   L. Wang, J. Pfeifer, C. Balázsi, I. M. Szilágyi, P. I. Gouma, Nanostructured hexagonal tungsten oxides for ammonia sensing. Proceedings of SPIE - The International Society for Optical Engineering "Nanosensing: Materials, Devices, and Systems III. 2007,6769:67690E.

[16]   C. Balázsi, K. Sedlackova, J. Pfeifer, A. L. Tóth, E. A. Zayim, I. M. Szilágyi, L. S. Wang, K. Kalyanasundaram, P. I. Gouma, Synthesis and examination of hexagonal Tungsten oxide nanocrystals for electrochromic and sensing applications. NATO Science for Peace and Security Series C: Environmental Security; Sensors for Environment, Health and Security. 2009:77-91.

[17]   J. Kukkola, M. Mohl, A. R. Leino, J. Maklin, N. Halonen, A. Shchukarev, Z. Konya, H. Jantunen, K. Kordas, Room temperature hydrogen sensors based on metal decorated WO$_3$ nanowires. Sens Actuat B. 186 (2013) 90-5.

[18]   Y. D. Zhang, W. W. He, H. X. Zhao, P. J. Li, Template-free to fabricate highly sensitive and selective acetone gas sensor based on WO$_3$ microspheres. Vacuum. 95 (2013) 30-4.

[19] C. Moreno-Castilla, M. A. Alvarez-Merino, F. Carrasco-Marín, J. L. G. Fierro, Tungsten and tungsten carbide supported on activated carbon: surface structures and performance for ethylene hydrogenation. Langmuir 17 (2001) 1752-6.

[20] A. Szymańska-Kolasa, M. Lewandowski, C. Sayag, G. Djéga-Mariadassou, Comparions of molybdenum carbide for the hydrodesulfurization of dibenzithiophene. CatalToday. 119 (2007) 7-12.

[21] A. Biedunkiewicz, A. Szymczyk, J. Chrosciechowska, Oxidation of (Ti,W)C ceramic powders. J Therm Anal Calorim. 77 (2004) 75-83.

[22] S. Kano, T. Inoue, Surface softening and hardening of WC-Co using pulsed laser irradiation. Surf Coat Tech. 201 (2006) 223-9.

[23] H. C. Kim, I. J. Shon, J. K. Yoon, J. M. Doh, Consolidation of ultra fine WC and WC-Co hard materials by pulsed current activated sintering and its mechanical properties. Int J Refract Metal Hard Mater. 25 (2007) 46-52.

[24] I. M. Szilágyi, J. Madarász, G. Pokol, F. Hange, G. Szalontai, K. Varga-Josepovits, A. L. Tóth, The effect of K^+ ion doping on the structure and thermal reduction of hexagonal ammonium tungsten bronze. J Therm Anal Calorim. 97 (2009) 11-8.

[25] L. Bartha, J. Neugebauer, Aspects of Effective Doping and the Incorporation of Dopant. Int J Refract Metal Hard Mater. 13 (1995) 1-34.

[26] E. Pink, L. Bartha, The Metallurgy of Doped/Non-Sag Tunsgten. London: Elsevier; 1989.

[27] I. M. Szilágyi, J. Madarász, G. Pokol, I. Sajó, P. Király, G. Tárkányi, A.L. Tóth, A. Szabó, K. Varga-Josepovits, J. of Thermal Analysis and Calorimetry. 98 (2009) 707-716.

[28] L. Bartha, B. A. Kiss, T. Szalay, Chemistry of tungsten oxide bronzes. Int J Refract Metal Hard Mater. 13 (1995) 77-91.

[29] Chemical Apparatus Engineering, company brochure, Plansee AG, Austria 2/97.

[30] E. Okorn, G. Leichtfried, in: Proc. 7th Int. Tungsten Symposium, Goslar, pp. 361-370, ITIA, London 1997.

[31] Tungsten-Based Products, company brochure, Ashot Ashkelon, Israel 11/92.

[32] Tungsten, company brochure, Plansee AG, Austria 3/95.

[33] W. H. Yih, C. T. Wang, Tungsten, Plenum Press, New York 1979.

[34] E. Lassner, in: Extractive Metallurgy of Refactory Metals, Proc. TMS-AIME 110th Annual Meeting 269-272, Chicago 1981

[35] V. Zbranek, Z. Zbranek, D. A. Burnham, US Patent 4.092400 1978.

[36] J. W. van Put, T. W. Zegers, A. van Sandvijk, P. J. M. van der Straten, in: 2nd Int. Conf. On Separation Science and Technology 387-394, C.S.Ch.E.M.H.I., Hamilton, Canada 1989.

[37] J. W. van Put, P. M. de Konig, A. van Sandvjik, G. J. Witkamp, in: Proc. 11th Symp. On Industrial Crystallization 647-652, Garmisch-Partenkirchen 1990

[38] I. M. Szilágyi, F. Hange, J. Madarász, G. Pokol, In situ HT-XRD study on the formation of hexagonal ammonium tungsten bronze by partial reduction of ammonium paratungstate tetrahydrate. Eur J Inorg Chem. 17 (2006) 3413-18.

[39] I. M. Szilágyi, J. Madarász, G. Pokol, P. Király, G. Tárkányi, S. Saukko, J. Mizsei, A. L. Tóth, A. Szabó, K. Varga-Josepovits, Stability and Contorlled Composition of Hexagonal WO3., Chem. Mater. 20 (2008) 4116-25

[40] T. A. Wilson, University of Illinois Bulletin, 1925, Vol. 23

[41] R. L. Prasad, A. Kushwaha, I. M. Szilágyi, L. Kótai, Solid state thermal degradation behaviour of 1-D coordination polymers of Ni(II) and Cu(II) bridged by conjugated ligand. J Therm Anal Calorim. 114 (2013) 653-64.

[42] I. M. Szilágyi, A. Deák, C. Várhelyi jr., J. Madarász, G. Pokol, Á. Gömöry, C. Várhelyi, Structural and thermal study of assymetric α-dioxime complexes of Co(III) with Cl and methyl-pyridines. Polyhedron. 10 (2010) 2185-9.

[43] M. Zumer, V. Nemanic, B. Zajec, M. Wang, J. Wang, Y. Liu, L. M. Peng, The Field-Emission and Current-Voltage Characteristics of Individual W_5O_{14} Nanowires., *J. Phy. Chem. Letters*. 112 (2008) 5250-5253.

[44] M. A. Dahlborg, G. Svensson, M. Valkeapää, The Structure of $Na_2W_2O_7.0,5H_2O$ Synthesized under High Pressure and Temperature. J. Sol. State Chem. 167 (2002) 525-533.

[45] B. A. Kiss, P. Gadó, J. A. Hegedűs, Az APT*5H2O termokondenzációjának vizsgálata termoanalitikai-infravörös spektrofotometriás és kiegészítő módszerekkel. Magyar Kémiai Folyóirat, 78 (1972) 30-38.

[46] S. Chandra, S. K. Topaldi, S A Hashmi, Experimental studies on the ionic (protonic) transport in APT*5H_2O. Journal of Physics:. Condensed Matter, 1 (1989) 9101-09.

[47] A. K. Basu, F. R. Sale, Characterizat.ion of various commercial forms of APT powder. Journal of Material Science, 10(1975) 571-577.

[48] A. Ogundipe, J. Pavlov, W. Braida, A. Koutsospyros, G. Sen, C. Christodoulatos, G. O'Connor, Evaluation of Analytical Methods to Address Tungsten Speciation, Global NEST Journal, 11 (2009) 308-317.

[49]   E. I. Ross-Medgaarden, I. E. Wachs, Structural Determination of Bulk and Surface Tungsten Oxides with UV-vis Diffuse Reflectance Spectroscopy and Raman spectroscopy, J. Phys. Chem. 111 (2007) 15089-99.

[50]   M. J. G. Fait, H. J. Lunk, M. Feist, M. Schneider, J. N. Dann, T. A. Frisk, Thermal decomposition of ammonium paratungstate tetrahydrate under non-reducing conditions Characterization by thermal analysis, X-ray diffraction and spectroscopic methods. Thermochim Acta. 469 (2008) 12–22.

[51]   J. Madarász, I. M. Szilágyi, F. Hange, G. Pokol, Comparative evolved gas analyses (TG-FTIR, TG/DTA-MS) and solid state (FTIR, XRD) studies on thermal decomposition of ammonium paratungstate tetrahydrate (APT) in air. J Anal Appl Pyrol. 72 (2004) 197-201.

[52]   S. A. A. Mansour, M. A. Mohamed, Thermal decomposition and the creation of reactive solid surfaces. V. The genesis course of the WO_3 catalyst from its ammonium paratungstate precursor. Thermochim Acta. 129 (1988) 187-96.

[53]   G. J. French, F. R. Sale, A re-investigation of the thermal decomposition of ammonium paratungstate. J Mater Sci. 16 (1981) 3427-36.

[54]   I. M. Szilágyi, J. Madarász, F. Hange, G. Pokol, On-line evolved gas analyses (EGA by TG-FTIR and TG/DTA-MS) and solid state (FTIR, XRD) studies on thermal decomposition and partial reduction of ammonium paratungstate tetrahydrate. Solid State Ionics. 172 (2004) 583-6.

[55]   I. M. Szilágyi, J. Madarász, F. Hange, G. Pokol, Partial thermal reduction of ammonium paratungstate tetrahydrate. J Therm Anal Calorim. 88 (2007) 139-44.

Tables

Table 1. Preparation conditions of WO_3 precursor powders by annealing APT or HATB starting materials, and the conditions of the solid-gas

phase reactions between the as-produced precursor powders and NH_3 and H_2O vapors

Entry Nr.	Preparing WO_3 precursor powders for the solid-gas phase reactions				Conditions of the solid-gas phase reactions			
	Starting material	Atmosphere	Temperature (°C)	Particle size (nm)	Precursor powder structure	Aqueous ammonia solution concentration	NH_3 pressure (kPa)	H_2O pressure (kPa)
1	APT	air	600	100-300	m-WO_3	13 M	43,40	1,37
2	APT	nitrogen	600	100-300	m-WO_3 partially reduced	13 M	43,40	1,37
3	HATB	air	600	70-90	m-WO_3	13 M	43,40	1,37
4	HATB	air	470	70-90	h-WO_3	13 M	43,40	1,37
5	APT	air	600	100-300	m-WO_3	0.1 M	0,15	2,34
6	APT	air	600	100-300	m-WO_3	1 M	1,56	2,28
7	APT	air	600	100-300	m-WO_3	0.5 M	0,77	2,32
8	APT	air	600	100-300	m-WO_3	6 M	12,23	1,97
9	HATB	air	600	70-90	m-WO_3	0.1 M	0,15	2,34
10	HATB	air	600	70-90	m-WO_3	1 M	1,56	2,28
11	HATB	air	600	70-90	m-WO_3	0.5 M	0,77	2,32

Figures
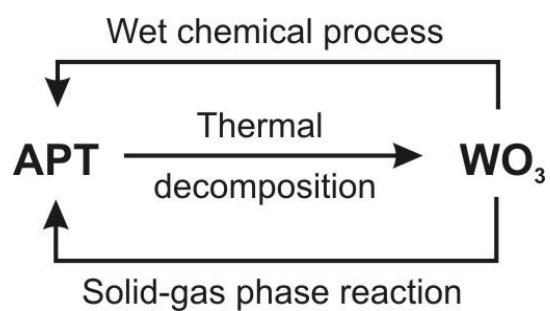
Figure 1. Scheme of the digestion experiment
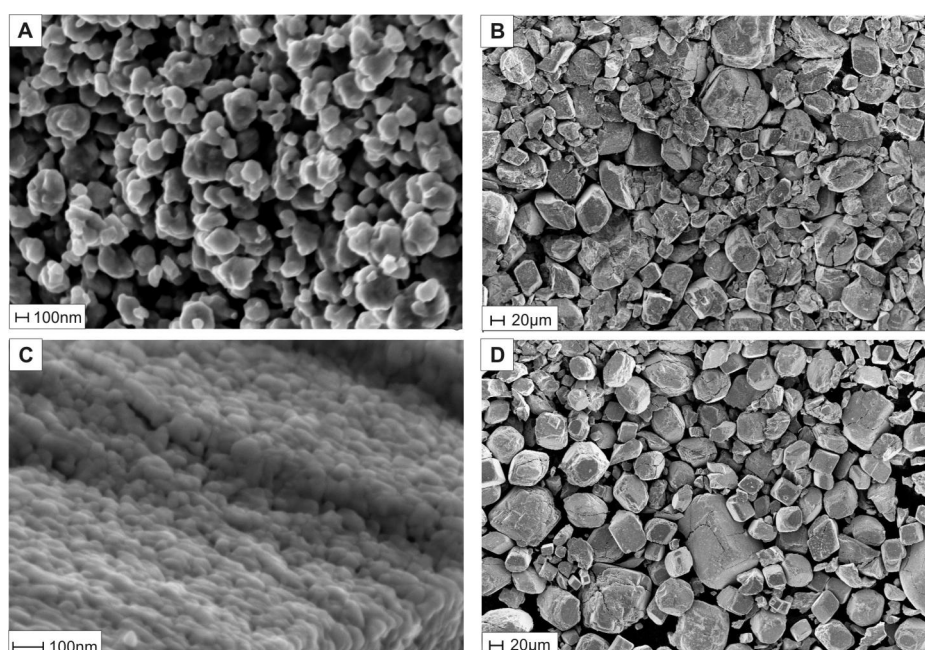
Figure 2. SEM images of the precursor oxides produced from APT (**1**, **2**, **5-8**) (a-b) and

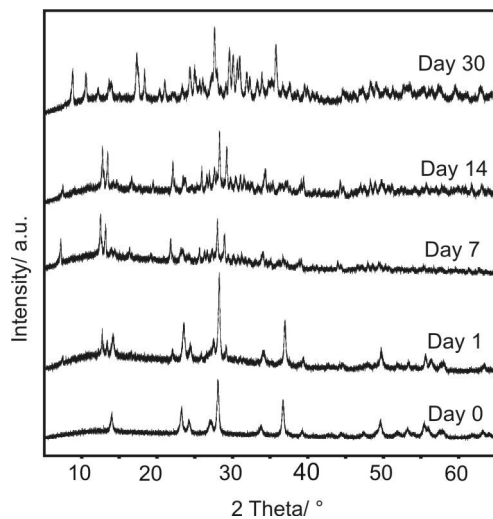HATB (**3**, **4**, **9-11**) (c-d)

Figure 3. XRD patterns of intermediate samples obtained from precursor **4** reaction at
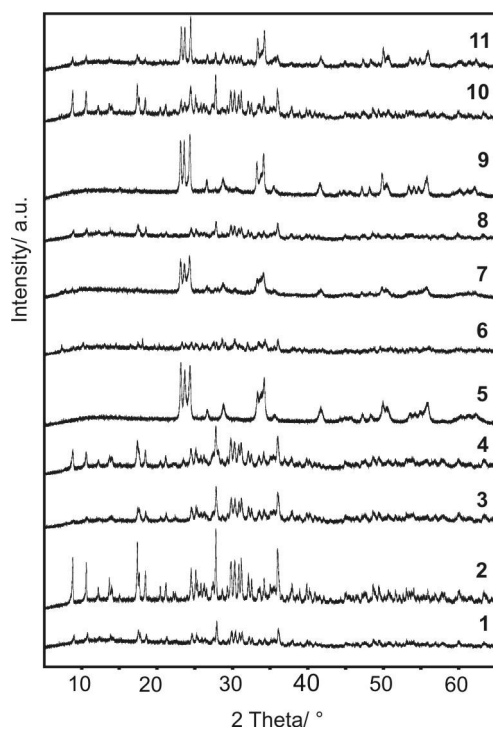
different reaction times

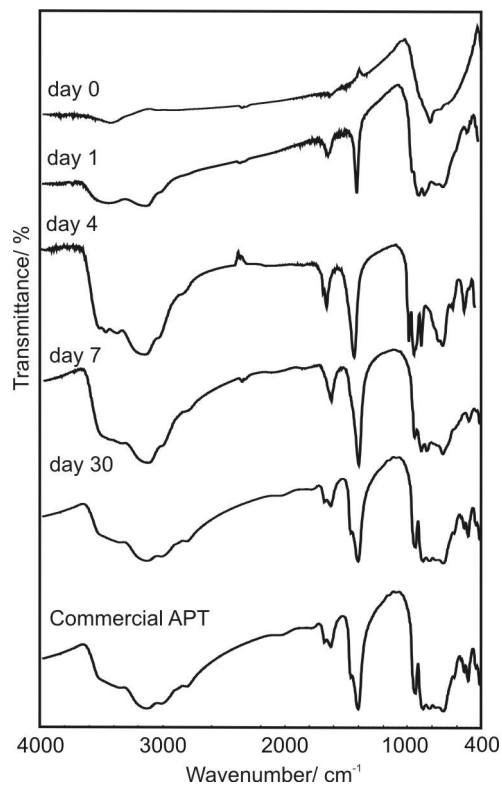Figure 4. XRD patterns of the reaction products after 30 days using precursors **1-11**

Figure 5. FTIR spectra of intermediate samples produced from precursor **2** reaction at

different reaction times
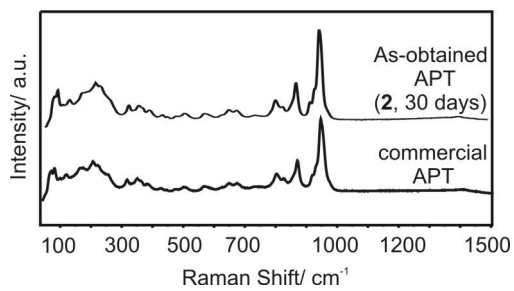
Figure 6. Raman spectra of the commercial and the as-obtained APT materials
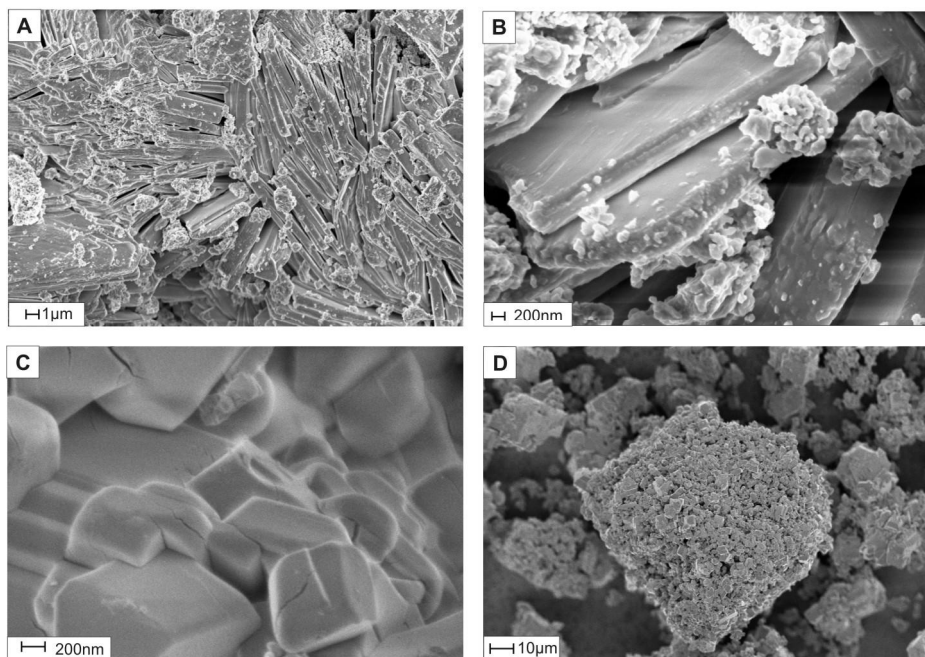
Figure 7. SEM images of partially reduced intermediate samples prepared from precursor **4**

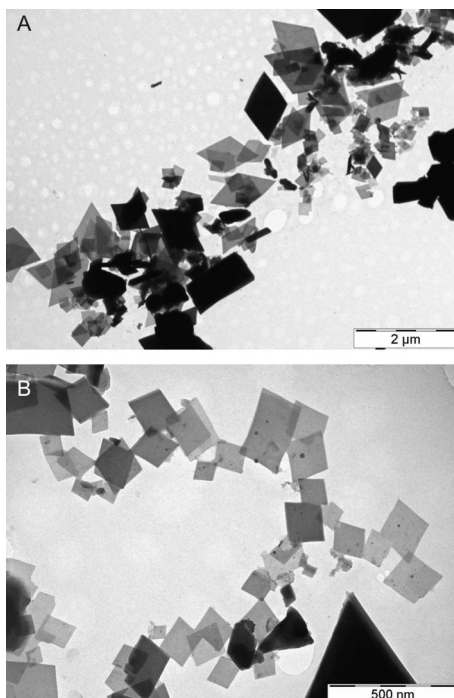after 7 days (a-b), and of APT produced from precursor **2** after 30 days (c-d)

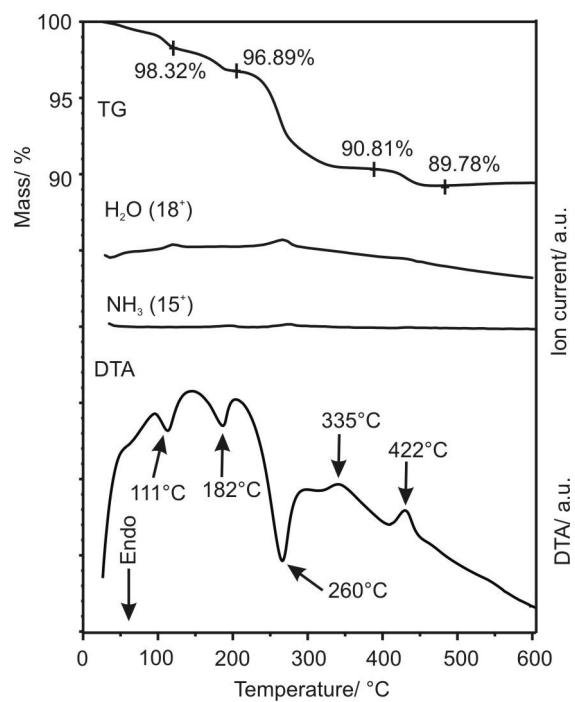Figure 8. TEM images of APT obtained from precursor **2**

Figure 9. TG/DTA and evolved gas analytical MS ion current curves in nitrogen of the as-obtained APT produced from precursor **2**